Revealing the Relative Electronic Landscape of Colloidal ZnO and TiO₂ Nanoparticles via Equilibration Studies

Janelle Castillo-Lora, *Ryoji Mitsuhashi, *, *and James M. Mayer*, *

- [‡] Department of Chemistry, Yale University, 255 Prospect St, New Haven CT 06520-8107 USA james.mayer@yale.edu
- [†] Current address; Department of Applied Chemistry for Environment, School of Science and Technology, Kwansei Gakuin University, 2-1 Gakuen, Sanda, Hyogo 669-1337 Japan

ABSTRACT: Interest in metal oxide semiconductors for energy processes has increased due to their prominent roles in photocatalysis, electrical energy storage, and conversion. However, an understanding of the thermochemistry of electron transfer (ET) reactions of these systems has lagged behind photophysical studies. This report investigates ET equilibria between reduced forms of well-characterized, ligated ZnO and TiO₂ nanoparticles (NPs) suspended in toluene. Multiple electrons were added to each type of NP, either photochemically or with a chemical reductant. Equilibration experiments monitoring these added electrons are used to construct a qualitative band diagram. Surprisingly, the difference between the 'reducible' oxide TiO₂ and the formally 'non-reducible' ZnO are reflected not in the relative band energies but rather in the relative width of the bands (the density of trap and/or band states). Moreover, the position of the electron equilibrium shifts upon addition of excess dodecylamine or oleic acid capping ligands. The directions of the equilibrium shifts suggest that they are due to the acid/base or hydrogen bond donor/acceptor properties of capping ligands. This suggests a coupling of protons with the electron transfers in these systems. These findings provide a more nuanced and detailed picture of ET thermodynamic landscapes at nanoparticles than what is provided in a typical nanoparticle band energy scheme. Aspects of this understanding could be valuable for the use of nanoscale oxides in energy technologies.

Introduction

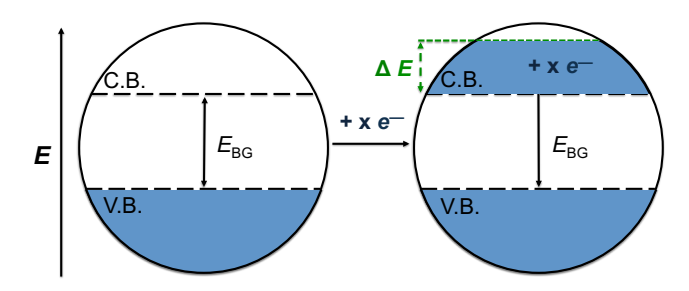
The study and use of metal oxide nanomaterials, such as TiO₂ and ZnO, have steadily grown over the last several decades. Electron transfer (ET) across the surface-solution interface is central to many of their applications. These include energy storage, solar energy conversion to electricity and fuels, self-cleaning surfaces, and catalysis.¹⁻⁴ While the spectroscopic properties of charge carriers in these materials have been studied in detail, much less is known about the thermochemistry of their ET processes. Greater understanding of the energetics of interfacial redox processes would be broadly valuable as electron transfer is central to many semiconductor applications.

A number of studies have examined the energies of the valence and conduction band edges of oxide semi-conductors, $E_{\rm VB}$ and $E_{\rm CB}$. These typically examined ET across an oxide/aqueous solution interface, and usually found a pH dependence of $E_{\rm VB}$ and $E_{\rm CB}$ of ca. 60 mV per pH unit. However, while the band gap energies are well known, there is significant variation in the reported $E_{\rm VB}$ and $E_{\rm CB}$ between these studies. A compendium of band energies for TiO₂ by Finklea shows a spread

of ± 0.5 V in the reported $E_{\rm CB}$ at each pH.⁶ For example, the detailed study of Enright and Fitzmaurice on both ZnO and TiO₂ electrodes gave a ~ 0.2 V lower potential for TiO₂,¹⁰ but the classic report by Grätzel shows them as being at the same energies.⁴

Studies of colloidal oxide nanoparticles (NPs) provide a direct way to look at the energetics of nanocrystal redox reactivity. Colloidal NPs are in some ways simpler than porous or dense thin films, for which diffusion of electrons, intercalants and electrolyte can be complicating factors. 10, 17-19 While direct measurements of reduction potentials for colloidal NPs are rare, a notable example is the direct electrochemical study of aqueous IrO₂ by Royce Murray and coworkers.²⁰ Gamelin *et al*. have recently developed an elegant potentiometric approach to examine the thermochemistry of non-aqueous ZnO and other colloidal NPs. 12-13 Equilibration between NPs has been shown to be a sensitive probe of relative energetics, between different materials, different sizes of the same NPs, different doping levels and other aspects of band engineering.²¹⁻²³

The electronic energy landscape of colloidal NPs is often depicted with simple, yet peculiar schematics such as in Scheme 1. The circles represent the physical shape of an idealized NP with superimposed energy parameters and band filling to indicate electrons, *i.e.* the Burstein-Moss Effect. 11, 24 While Scheme 1 nicely illustrates some aspects, there are many other important factors that influence the NP the electronic energy landscape, such as size, 22, 25 doping, 21 capping ligands, 26-30 solvent and pH. 5,6 From this perspective, redox reactions at the nanoscale have some characteristics of molecular redox chemistry as well as bulk surface-solution processes.



Scheme 1: Left: Rough schematic of the valence and conduction bands (VB and CB) of a semiconducting NP and the energy of the band gap, with the circle standing for the physical shape of an idealized NP. Right: filling of a NP with extra electrons.

Scheme 1 also shows that the energetics can be strongly affected by the amount of band filling. The energetic change upon band filling is formally a capacitance¹² and should also reflect the density of states (DOS) in the ensemble of colloidal NPs. The DOS in films of nanoscale TiO2 has been extensively examined.31-33 The DOS is typically assumed to be exponential with energy, though that is not always the case. Other factors that also need to be considered include morphology, pH etc. It has become generally clear that "electron accumulation is accompanied by adsorption/insertion of cations (mainly protons) for charge compensation."31 This is also indicated by the longknown Nernstian pH dependence of oxide semiconductor band edge energies.⁵, 14, 34-36 In our view, this coupling of electrons and cations requires that the energetics must include the cation binding, not purely the electronic energies. In regards to small ZnO NPs, there has been a lesser focus, with the notable exception of recent studies of charging colloidal ZnO NPs. 12-13, 22, 25, 34-35, 37-38 The presence of quantum confinement has suggested the presence of discrete quantized states within the band,³⁹ although this may not be evident in an ensemble with a distribution of sizes.

The study described here uses an equilibration methodology as a very sensitive probe of the relative energetics between ZnO and TiO₂ NPs. Charge transfer between the NPs has been studied as a function of band filling and capping ligand concentrations. Well-defined dodecylamine-capped ZnO and oleate-capped TiO₂ colloidal

nanoparticles (NPs) were independently synthesized and reduced by many electrons. These reduced colloids are stable over months and can be easily studied via optical and EPR spectroscopies.⁴⁰

This study provides an understanding of the electronic landscape of multiply charged nanomaterials, considering properties both internal and external to the NPs. Electron equilibration experiments confirm that the E_{CB} of nanoscale ZnO vs. TiO2 are very similar, as previously reported.^{4, 10} However, the experiments show that the density of states in TiO₂ is *much larger* than that of ZnO. This is the origin of the general perception that TiO₂ is a reducible oxide while ZnO is not. In addition, the studies with added ligands indicate the coupling of redox energetics with the acid/base properties of the solution, even in low polarity organic media. This is consistent with studies from our lab and others that have shown the explicit influence of protons and cations on the effective reduction potentials of ZnO and TiO₂ NPs.³⁶ The noninnocent effects of surface ligands, which are traditionally consider only as stabilizing agents, is another important component of redox thermochemistry of these very common nanomaterials.

Experimental Section

Synthesis and Characterization. All experiments, unless otherwise noted, were carried out in toluene under an N_2 atmosphere. Dodecylamine (DDA)-capped ZnO ($d=3.7\pm1.0$ and 5.6 ± 1.0 nm; 1000-4000 Zn atoms) and oleate (OL)-capped TiO₂ ($d=4.5\pm1.5$ and 4.8 ±1.5 nm; 1500-2500 Ti atoms) nanoparticles (NP) were synthesized and characterized as previously reported.⁴¹⁻⁴²

Reduced TiO₂ and ZnO nanoparticles (e^-/TiO_2 and e^-/ZnO) were prepared by UV irradiation (100 W Hg lamp) in the presence of ethanol. The reduced NPs were marked by a blue coloration and possessed distinct optical signatures. The electrons in reduced ZnO (e^-/ZnO) have a very broad near IR absorption with a substantial tail in the visible region, while e^-/TiO_2 exhibits a broad peak at 700 nm. The time course of TiO₂ and ZnO photochemical reduction was followed by optical spectroscopy for 2 hours, after which the absorbance feature leveled out signifying maximum reduction. The generation of these extra electrons were also confirmed with EPR spectroscopy, by the distinct isotropic (g = 1.96) signal for e^-/ZnO and the axial ($g_{\perp} = 1.92$ and $g_{//} = 1.91$) signal for e^-/TiO_2 .

The electron concentrations of ZnO and TiO₂ NPs in solution were determined by anaerobic titration with 2,4,6-tri-*tert*-butylphenoxyl radical (ArO•) as previously described (Figure S1).⁴⁰ The linear dependence of e^-/MO_x absorbance on electron concentration (mol e^-/L) from the titrations showed that the Beer-Lambert law was followed throughout the examined spectral range. The molar extinction coefficients obtained from the

slopes of the titration data (i.e. $\epsilon_{600 \text{nm}} = 700 \pm 70$ for e^-/TiO_2 and $\epsilon_{850 \text{nm}} = 1000 \pm 100$ for e^-/ZnO) are independent of the concentration of NPs and agree with previously published results. The availability of molar extinction coefficients for each of the NPs at different wavelengths allowed determination of the concentration or number of electrons on both NPs, for both chemically and photochemically reduced samples (SI Equation 1). Dividing this by the NP concentration afforded the number of electrons per NP. Photochemical reduction yielded 150 e^- per TiO₂ NP, 5 e^- per large 5.6 nm ZnO NP, and 3 e^- per small 3.7 nm ZnO NP. The $\pm 10\%$ uncertainty in the molar extinction coefficient values is the primary uncertainty in these studies and applies to all values reported here.

Chemical Reduction Experiments. Chemical reduction studies were typically performed by titrating the outer-sphere chemical reductant, decamethylcobaltocene $(CoCp^*_2, E_{1/2} = -1.9 \text{ V vs. Fc/Fc}^+ \text{ in THF})$ into a solution of diluted uncharged NPs.³⁵ Chemical reduction involved the formation of e^{-}/MO_x with a tightly ion-paired CoCp*₂ since reactions were performed in low-polarity toluene. NP reduction resulted in the growth of the same optical features as photochemical reduction, and maximum reduction was indicated by both peak formation at 350-400 nm attributable to CoCp*2 and a lack of optical change in the visible region (Figure S2). Typically, 0.01 mM ZnO was treated with excess reductant resulting in 1-3 e^- per ZnO, depending on size. A solution with 0.01 mM TiO₂ was also treated with excess CoCp*₂ and was reduced to $90 e^{-/\text{TiO}_2}$.

Interparticle Electron Equilibration Experiments. Studies of ET between ZnO and TiO_2 nanoparticles were performed and monitored primarily by optical and EPR spectroscopies. In a typical UV-Vis study, a solution containing 0.2 mM e^- on 0.002 mM of TiO_2 NPs (TiO_2) was titrated with 0.02 mM of uncharged 5.6 nm ZnO NPs, corresponding to a 10:1 ratio of ZnO: TiO_2 NP (excess ZnO stoichiometry explained below), and monitored in a quartz cuvette at room temperature. Changes in the optical spectrum were monitored and quantified to determine the number of electrons on either ZnO or TiO_2 at equilibrium. This protocol is similarly performed when analyzing how capping ligands perturb equilibrium.

ET reactions were also monitored by EPR spectroscopy and performed similarly. Typically, a solution composing 0.5 mM e^- on 0.005 mM of TiO₂ NPs (100 e^- /TiO₂) were treated with 0.1 mM ZnO NPs. Samples were flash frozen at various time points and measured at 7K (Figure S3). Analysis to determine whether electrons had completely or partially transferred from TiO₂ re-

quired fitting the EPR spectrum as either a single (electrons on ZnO only) or a multi-component system (electrons on TiO₂ and ZnO) (Figure S4).

Table 1. Differences in reduction level based on charging method and NP profile a

NP		Carrier density ^b	e ⁻ /M ⁺	e ⁻ /NP from CoCp* ₂	e ⁻ /NP from TiO ₂
TiO ₂	150	10^{21}	8%	90	N/A
ZnO 5.6 nm	5	1019	0.08%	3	7
ZnO 3.7 nm	3	10^{19}	0.07%	1	4-5

^a Charging by UV irradiation in the presence of ethanol (hv), or by electron transfer from $CoCp^*_2$ or e^-/NP . ^b Carrier density in e^-/cm^3 .

Results

I. Approach to quantifying electrons in nanoparticle containing reaction mixtures.

Different reduction methods of the two types of nanoparticles led to a range of maximum number of electrons per nanoparticle (Table 1). These experiments involved colloidal ZnO and TiO₂ NPs that are roughly the same size (d=3.7-4.5 nm) with similar extinction coefficients per electron from 400-900 nm. In contrast to these similarities, a TiO₂ NP is able to hold 30-50 times more electrons than a ZnO NP of equivalent size. Responding to this large difference in e^-/NP , the equilibration experiments described below were done with much higher concentrations of ZnO NPs than TiO₂ NPs (concentration = moles of NPs/L). This allowed the *concentration of electrons* on TiO₂ NPs (moles of e^-/L) to be similar to the electron concentrations on ZnO.

The interparticle experiments below are typically described with the metric of percent electrons on TiO₂ or ZnO (% e^- _{TiO²/ZnO}). This is an accessible way to describe where electrons have transferred and equilibrated. The electron per NP (e^- /NP) notation is also used and provides a more nuanced view of the reduction of each nanoparticle. In a hypothetical example, 150 e^- can be held in a single TiO₂ NP, whereas dozens of ZnO NPs would be needed. Ultimately, the experiments below reveal the reasons why the maximum number of electrons is different between ZnO and TiO₂ and how the respective NP reactivity is impacted.

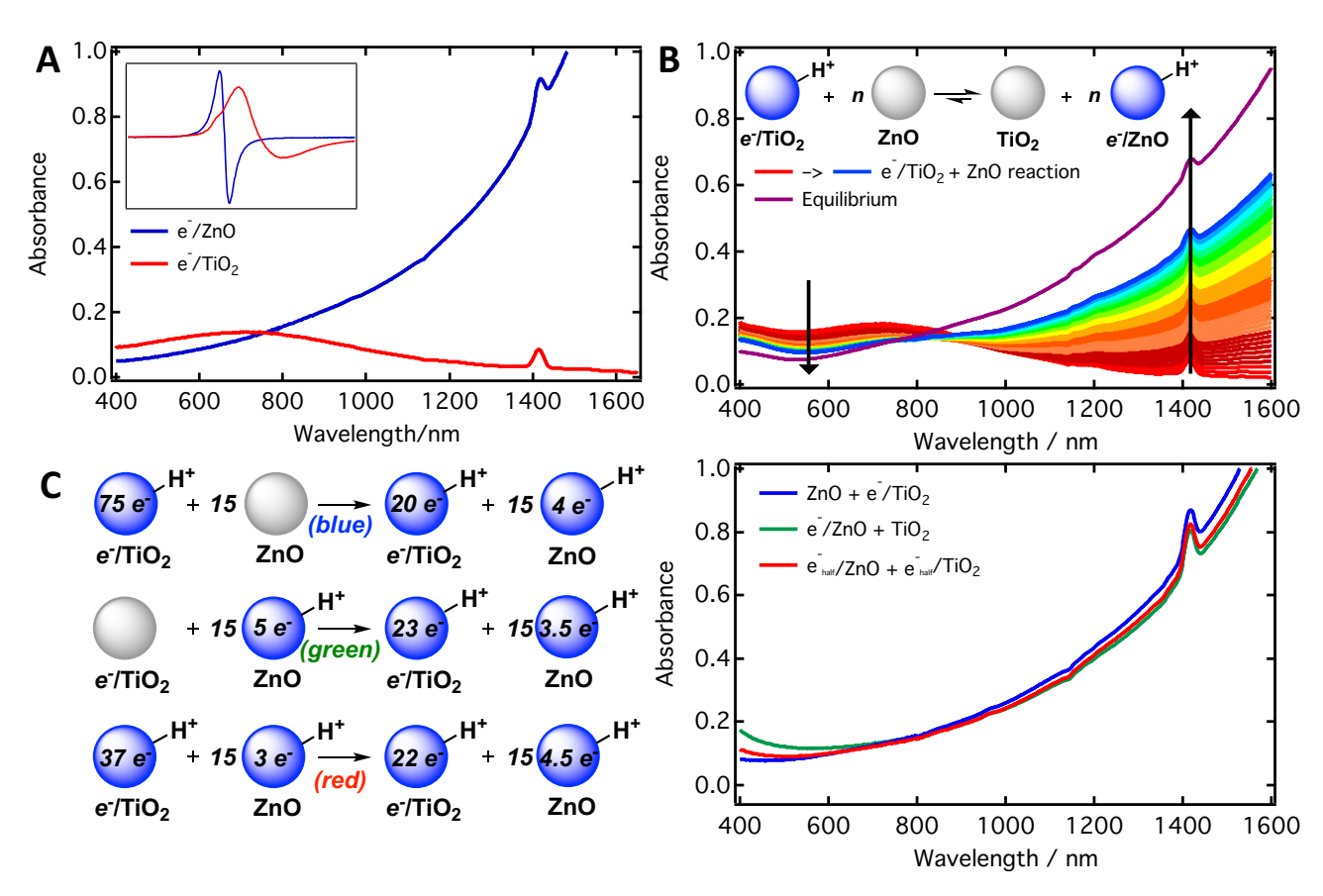


Figure 1: Optical and EPR (inset) characterization spectra of 0.2 mM electrons on ZnO (blue) and 0.2 mM electrons on TiO₂ (red). The small peak at ∼1420 nm is attributable to an overtone from residual ethanol from the synthesis. An expanded version of the EPR spectrum is given in Figures S3A. Uncharged, as-prepared NPs do not have absorption signatures within the indicated range of the optical and EPR spectra. (B) Optical spectra time course of a reaction between reduced TiO₂ NPs and ZnO NPs in toluene. The red-to-blue change (indicated by black arrows) required 30 mins; the final unchanging spectrum (purple) was obtained at 3 h. (C) Left: Reactions probing interparticle ET equilibrium. Right: Optical spectra of the reactions after reaching equilibrium (3 hours). Regardless of whether the electrons originated on TiO₂, (blue), ZnO (green), or both (red), the same spectrum (Right) and electron distribution was obtained, indicating an equilibrium process.

II. Equilibrium processes at ZnO and TiO₂ NPs: relative densities of states and electron energies.

A. Equilibration with CoCp*2

The relative reduction of TiO₂ and ZnO NPs is measured via equilibria studies with CoCp*2; optical spectra affords the number of electrons on ZnO or TiO2 (Figure 1A). As previously described, addition of excess CoCp*₂ to DDA-capped ZnO caused significant reduction of the NP resulting in 3 e⁻ per 5.6 nm diameter ZnO NP.³⁶ Similar results were seen with OL-capped TiO₂ NPs in toluene; reduction with CoCp*2 yielded significant more reduction of the NPs resulting in 90 e per TiO₂ NP. Multiple experiments with excess CoCp*₂ consistently showed this large difference, that one TiO2 NP was reduced by 30 times more electrons than one 5.6 nm ZnO NP. When the number of ZnO and TiO₂ NPs is adjusted such that there are equal numbers of TiO2 and ZnO "sites for reduction" (i.e. 0.003 mM TiO2 and 0.1 mM ZnO), both solutions showed a maximum charging of ~ 0.3 mM e^- upon addition of excess CoCp *_2 . These studies show that in order to have the same number of electrons on each particle, the concentration of ZnO needs to be 30 times greater than TiO₂. As previously mentioned, size may also affect how band filling occurs.³⁶ Smaller 3.7 nm ZnO NPs afford 100 times more electrons on TiO₂ than ZnO (Figure S2), implicating size effects in the equilibrium process with CoCp*₂.

B. Interparticle ZnO/TiO₂ equilibrations

The chemical reduction experiments described above initially appear to show that TiO_2 is much more easily reduced compared to ZnO. However, to truly compare the relative energies of many electrons (past the bottom of the band or the lowest trap state), interparticle electron transfer equilibrium reactions were performed to understand the flow of electrons between TiO_2 and ZnO. For instance, the addition of e^-/TiO_2 to uncharged ZnO resulted in substantial ET to the ZnO, as demonstrated by optical (Figure 1B) and EPR spectra.

In one experiment, three separate cuvettes contained identical numbers of ZnO NPs, TiO₂ NPs, and total electrons, differing only in the original placement of the electrons. Specifically, the electrons were initially either

all on ZnO, all on TiO₂, or distributed between both NPs (Figure 1C). Monitoring the equilibration of electrons upon addition of uncharged ZnO to $e^-/{\rm TiO_2}$ showed substantial ET from TiO₂ to ZnO, similar to Figure 1B. The reverse direction (uncharged TiO₂ to $e^-/{\rm ZnO}$) did not result in a dramatic change. Mixing $e^-/{\rm ZnO}$ and $e^-/{\rm TiO_2}$ with the same total electron concentration gave the same equilibrium distribution: 75% of the electrons were on ZnO (3.5 $e^-/{\rm ZnO}$) and 25% were on TiO₂ (~21 $e^-/{\rm TiO_2}$) (<5% RSD) (Figure 1C). A parallel experiment was done using EPR spectroscopy (Figure S3). After 1.5 hours, the resulting spectra were again very similar, further demonstrating that these are equilibrium properties.

The equilibration experiments above show the behavior of the most reducing electrons in the ZnO and TiO_2 NPs, near the *top* of their energy distribution. Specifically, the electrons in TiO_2 are higher in energy (more reducing) than most of the states in the CB of the ZnO. This is shown by the transfer of most of the e^-/TiO_2 to ZnO, while few e^- transfer from e^-/ZnO to TiO_2 .

Experiments were also done to probe whether the lowest energy of ZnO and TiO2, the states near the conduction band edge or in traps, are of similar energy as commonly reported in the literature. 4, 10 Excess ZnO was added to e^{-}/TiO_2 to push the equilibrium to completely oxidize TiO_2 . A solution containing $100 e^{-}/TiO_2$ NP was treated with aliquots of uncharged 5.6 nm ZnO NPs. Even at the first aliquot (10:1 ratio of ZnO:TiO₂ NP), there was a dramatic change in the optical spectrum, indicating substantial ET from e^{-}/TiO_{2} to ZnO (analogous to Figure 1B). Subsequent addition of ZnO (37:1 ZnO:TiO₂ NP) resulted in small changes in the electron distribution ratio or e^{-}/ZnO to e^{-}/TiO_2 . Despite the excess of 5.6 nm ZnO NPs, the optical spectra showed that $20\% \pm 10\%$ of electrons still remained on TiO₂. This shows that the lowest energy TiO₂ states are lower than the bottom of the ZnO band.

A similar experiment using an excess of smaller 3.7 nm ZnO NPs showed that $33\% \pm 8\%$ of electrons remained on TiO₂ (Figure S5). These results affirm the previous experiments showing that the predominant electron flow is from e^-/TiO_2 to ZnO. Again with these NPs, the 33% electrons remaining on TiO₂ demonstrate that the lowest electrons on TiO₂ that occupy states that are lower in energy than the bottom of the ZnO band. The presence of more electrons remaining on the TiO₂ with smaller ZnO NP reflects the known raising of the ZnO CB energy due to quantum confinement. ^{22, 41, 43}

These sets of experiments overall demonstrate three important results. First, interparticle ET is an equilibrium process, reaching the same equilibrium state regardless of where e^- originate. Secondly, the preferential flow of most of the electrons is from TiO_2 to ZnO, suggesting that TiO_2 is, under most conditions, more reducing. However, under some conditions, TiO_2 can also be more oxidizing. These measurements thus provide a

much more detailed view of the relative energetics than the many prior experimental and computational studies that reported conduction band edge energies of ZnO and TiO₂.

III. Ligand and acid/base effects on interparticle electron transfer

Capping ligands are widely used in colloid chemistry in organic solvents to stabilize NP suspensions; they have also been shown to impact the energetics and optical properties of NPs.²⁶⁻²⁷ Colloidal NP suspensions contain significant amounts of unbound ligands. Since these capping ligands have reactive functionalities, including acidic and basic moieties, understanding how the native ligands can influence the thermodynamics of the NPs is important.

The NPs used in this study were synthesized in a consistent fashion to minimize any differences in capping ligand coverage. For the ZnO stock solutions used in the equilibration experiments described below, integration of the DDA ¹H NMR signal showed ~5.4 mM DDA. This corresponded to 120 total ligands per ZnO NP in the suspension. Prior work from our lab used such NMR spectra to show that NPs had roughly equal amounts of strongly-bound, weakly-bound and free (unbound) DDA molecules. This corresponds to ≤25% surface coverage, even including the highly labile weakly bound ligands.⁴⁴ The TiO₂ NP colloids used here contained ca. 60 mM (bound and unbound) total oleate (OL)/oleic acid (OL-H) (1000 ligands per NP) in the stock solution. The ¹H NMR spectra show resolvable signals for the vinyl protons of bound ligands on the TiO2 NPs versus the free ligand in the toluene solution (Figure S7).⁴⁵ This analysis indicates ~60% surface coverage for TiO₂. Thus, the TiO₂ NPs have a much higher coverage of surface oleate ligands compared with the coverage of DDA on the ZnO

Initially, uncharged ZnO was treated with 6 eq. $CoCp^*_2$ to yield 3.5 e^-/ZnO (2.5 eq. of unreacted $CoCp^*_2$ at equilibrium). This solution also contained 0.55 mM DDA (diluted 10-fold from the stock solution). The addition of excess DDA to solution led to an increase in absorbance at 400-500 nm. These changes indicate ET from e^-/ZnO back to $CoCp^*_2^+$ to form $CoCp^*_2$. In the new equilibrium state, the number of electrons per ZnO decreased to from 3.5 to 2 e^-/ZnO (Figure 2A).

In contrast, addition of a large excess of 70 mM OL-H, the non-native ligand, to the equilibrated $ZnO/CoCp^*_2$ suspension gave an initial increase in the absorbance at >800 nm, indicating 6 e^-/ZnO . Since there were only 6 eq. of $CoCp^*_2$ present at the outset, the addition of the acid shifted the equilibrium sufficiently that all of the electrons transferred from the reductant.

Following the initial increase in ZnO reduction, a slower secondary decrease in absorbance was observed

over the course of several minutes (Figure 2A). This secondary decrease absorbance was coupled to a slight blueshift in the ZnO band edge absorbance. These spectral changes are consistent with the partial dissolution of ZnO to soluble zinc oleate and subsequent shrinkage of the NPs (Figure S8). Dissolution of ZnO by oleic acid reduces the size of the particles and therefore transfers electrons back to CoCp*2+. Such dissociation of M(OL)2 and related species has been observed with chalcogenide NPs. Rn This illustrates that there is some exchange of ligands, with ZnO binding some oleate, with displacement of some of the native DDA ligands. The ligand exchange likely contributes to the effects observed.

Similar overall trends were observed with TiO₂. Initially, an equilibrated suspension of TiO₂ NPs with 2 mM OL/OL-H and 60 eq CoCp*₂ yielded 51 *e*⁻/TiO₂ (diluted from stock solution). Ten times lower TiO₂ NP concentration was used in this study compared to the ZnO case, due to the ability of each TiO₂ to hold many more electrons. Addition of the same large excess of OL-H to reach 70 mM caused the number of *e*⁻ per NP to increase to 55 *e*⁻/TiO₂, leaving 5 eq. of CoCp*₂ unconsumed. Similarly, addition of 80 mM DDA resulted in a decrease down to 23 *e*⁻/TiO₂ (Figure 2B). Therefore, both ZnO and TiO₂ NPs equilibrated with CoCp*₂ showed an increase in the number of electrons on the NPs with OL-H addition but a decrease with added DDA.

An equilibrated suspension of both reduced ZnO and TiO₂ NPs was prepared, containing 75% of the e^- on ZnO (9 e^- /ZnO) and 25% e^- on TiO₂ (25 e^- /TiO₂) (Figure 2C). This mixture contained 2 mM OL/OL-H and 0.50 mM DDA. Addition of excess OL-H to bring the concentration of OL/OL-H to 30 mM caused a shift in the optical spectra. The spectra indicated the transfer of 15% of the

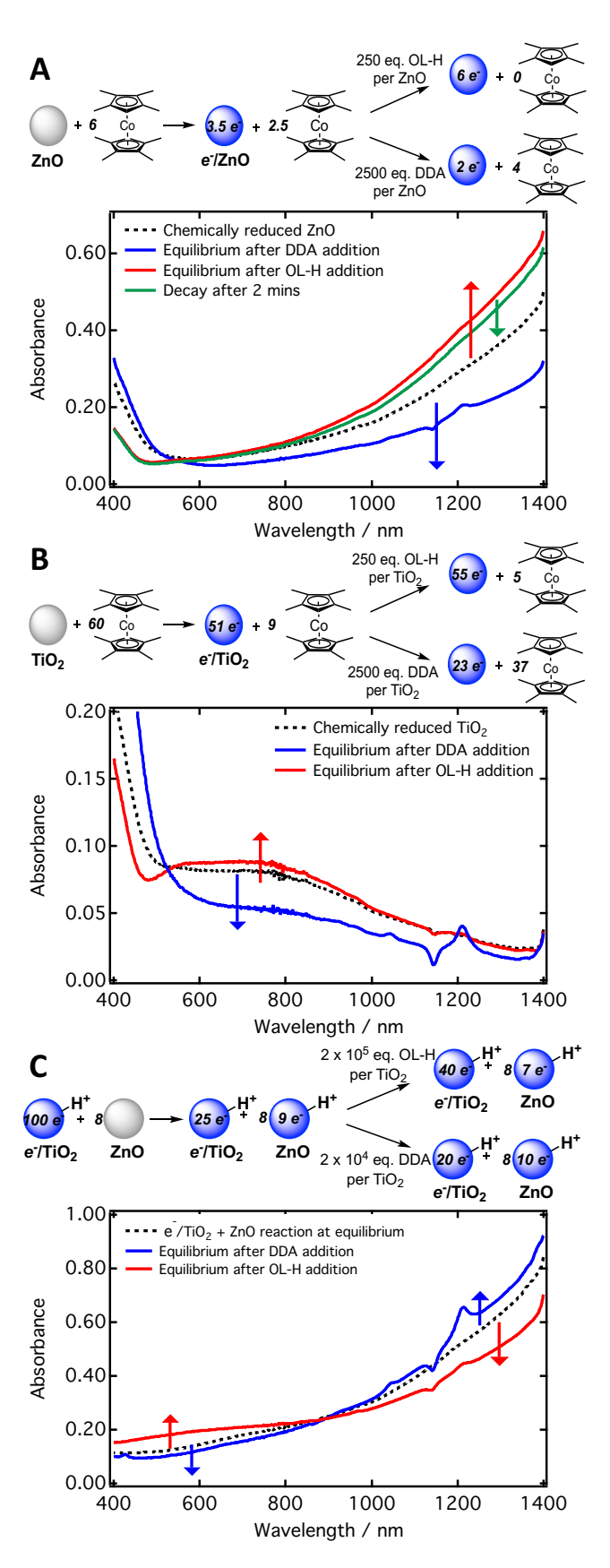


Figure 2. Optical spectra showing perturbation of initially equilibrated ET reactions (black dashed lines) upon addition of DDA or OL-H. The absorption at 1150 nm is attributable to a THF overtone. (A) Addition of DDA to an equilibrated ZnO/CoCp*₂ suspension resulted in fewer elec-

trons on ZnO and an increase in $CoCp^*_2$ (less absorption in the NIR and increased intensity below 500 nm, blue). OL-H addition caused the NIR absorbance to initially increase indicating more e^- on ZnO (red) but then decreases over minutes (green). Note that charge-balancing surface bound $CoCp^*_2$ are omitted for clarity. (B) Addition of OL-H to an equilibrated $TiO_2/CoCp^*_2$ suspension caused an increase in the broad visible absorption, indicating more e^-/TiO_2 , until the reductant is completely consumed (red). DDA addition caused a decrease in absorption and the e^-/TiO_2 (blue). In the schematic equations, the charge-balancing surface-bound $CoCp^*_2$ are omitted for clarity. (C) Addition of OL-H caused ET from ZnO to TiO_2 (red) while added DDA caused the opposite change (blue).

electrons from ZnO to TiO₂, yielding a new equilibrium position where there were $60\%~e^-$ on ZnO ($7~e^-$ /ZnO) and $40\%~e^-$ on TiO₂ ($40~e^-$ /TiO₂). Addition of excess DDA to a separate aliquot of the equilibrated suspension, to reach 250 mM DDA, showed a change in the opposite direction, with ET from TiO₂ to ZnO. The fraction of electrons on ZnO increased to $80\%~(10~e^-$ /ZnO) with the corresponding decrease yielding $20\%~e^-$ on TiO₂ ($20~e^-$ /TiO₂) (Figure 2C). Similar results were obtained using a sample of reduced ZnO that had been synthesized with one less washing step and therefore had excess DDA. Using these NPs, there was complete transfer of electrons from TiO₂ to ZnO (Figure S10).

Discussion

The storage of multiple redox equivalents in an individual nanoparticle is important for many applications, such as in H₂O splitting or CO₂ reduction. In one instance, Grätzel and coworkers showed that colloidal TiO_2 can undergo substantial band filling ($10^{20} e^{-/cm^3}$) for potential use for such reactions.⁴⁷ In our studies, ZnO and TiO₂ have been demonstrated to be able to be doped to high charging levels, with 3-5 e⁻ per 3.7-5.6 nm diameter ZnO NP ($10^{19} e^{-/\text{cm}^3}$) and dozens of electrons in each TiO₂ NP (10²¹ e⁻/cm³). Despite similar NP sizes and electron molar extinction coefficients, a large discrepancy in charging is evident. Probing the nature of these electrons and their charge-balancing protons requires a model that goes beyond the commonly used one-electron schematic representative of the conduction band edge. Such a model needs to include information about band or trap state filling and how the solution media affects the redox states.

The next section uses the equilibration results to develop a qualitative model that describes the relative filling of the CBs in the two materials upon reduction. The following sections then discuss the different ways that this model is incomplete, to provide a more fine-grain description of redox reactions involving oxide NPs.

I. Building a relative density of states model

The equilibration studies provide several insights into the relative density of states (DOS) for electrons added to ZnO and TiO2 NPs. Prior studies of reactions involving ZnO NPs, CoCp*2, and acids/cations demonstrate strong evidence that thermal reactions at NPs stop changing when a thermodynamic equilibrium is reached. In these reduced NP systems, equilibrium occurs when the energies of the highest energy electrons are equal.³⁴, ³⁶ Interparticle ET equilibrium is demonstrated by the consistent final electron distributions obtained for the same e⁻/ZnO/TiO₂ mixture regardless of which NP the electrons originated (Figure 1C). In the equilibrations with CoCp*₂, the highest energy electrons are equal and set by the potential of the reductant (Figure 2A, 2B).⁴⁸ We note that the syntheses of ZnO and TiO2 were kept consistent to minimize differences in capping ligand coverage (see the next Section).

Chemical reduction experiments demonstrate a large difference in the maximum number of electrons per NP upon reaching equilibrium with $CoCp^*_2$: there are 30 times more electrons in each TiO_2 NP than in a ZnO NP. This indicates that the integrated number of occupied states is 30 times larger for each TiO_2 NP than for each ZnO NP at the electron energy set by the $CoCp^*_2$ +/ $CoCp^*_2$ redox couple.

The interparticle ET equilibration experiments show that the predominant electron flow is from $e^-/\text{Ti}O_2$ to ZnO, in experiments with a 10-15-fold excess of ZnO NPs to TiO₂ NPs. Thus, the majority of the electrons on the TiO₂ NPs are at higher energy than the states in the ZnO NPs. However, excess uncharged ZnO removed only a portion of the electrons on $e^-/\text{Ti}O_2$. This behavior is different than the mass-action equilibrium expression that would be observed for a molecular electron transfer. It indicates that the lowest energy ZnO states are higher than the lowest energy TiO₂ states.

Rationalization of these results requires first a discussion of the specific states on each NP and the nature of the colloidal system. Electrons in TiO2 NP are widely regarded to occupy a distribution of trap states of varying structures and energies. 7-8, 49-52 This is how EPR spectra similar to that in Figure 1A inset have typically been interpreted.⁵² This implies that the states in an individual NP are better described as a set of discrete orbitals rather than as a true band. Electrons added to ZnO NPs such as used here have been shown to occupy orbitals that are delocalized over the whole NP and have quantum-confined properties in the small NPs. 25, 53-54 The quantum-confinement means that these orbitals also have discrete energies rather than forming a continuous band. Thus, while the nature of the orbitals is different in TiO₂ and ZnO, within a single NP these are both best described as an ensemble of discrete states.

The schematic diagram in Figure 3A represents these states side-by-side for a TiO₂ NP and a ZnO NPs in equi-

librium with excess CoCp*2. In this picture, the vertical axis is energy and the short horizontal lines represent the states in each NP. The dashed line represents the energy of electrons at the CoCp*2+/CoCp*2 potential, such that states lower in energy are occupied (red) and those higher are empty (blue). The horizontal width represents the average or integrated number of states at the specified energy. The number of states in a given energy band rises with energy, as is typical. The states in a 4.5 nm TiO₂ NP are represented by the broad distribution at left, while narrow set of states describes a 5.6 nm ZnO NP. The different widths are indicated by the ability of TiO₂ to be reduced 30 times more than ZnO, indicating that each TiO2 must have 30 times as many states as each ZnO NP below the potential of CoCp*2. In addition, there must be TiO₂ states below the ZnO states because the ZnO NPs are unable to fully oxidize the TiO₂ NPs.

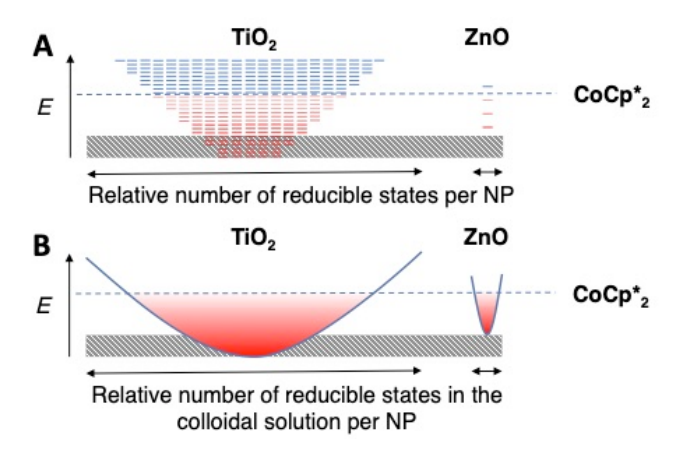


Figure 3. Schematic depiction of electron band filling in a TiO₂ NP versus a single ZnO NP upon equilibration with CoCp*₂. Red coloring is indicative of states occupied by electrons whereas the blue coloring indicates empty states. (A) Depiction of the density of individual states (horizontal lines) in a single NP: trap states for TiO₂ (left) and quantum-confined states for ZnO (right). (B) Depiction of the density of states in an ensemble of NPs in a colloidal suspension, with the broader band of TiO₂ trap states (left) contrasting with the narrow band of quantum-confined states for ZnO (right). Chemical reduction experiments consistently resulted in TiO₂ possessing 30x more *e*⁻ than ZnO. Additionally, the lowest TiO₂ states are lower than the lowest ZnO states, as addition of excess ZnO does not result in complete TiO₂ oxidation.

While Figure 3A represents the electronic structure for individual NPs, the actual equilibration experiments reflect the total DOS in the colloidal suspension as a whole. This is an ensemble of (typically) 2 μ M TiO₂ NPs and 20 μ M ZnO NPs (10^{15} - 10^{16} NPs per mL). The ensemble contains a distribution of particle sizes and shapes, and therefore a distribution of trap state and quantum-confined state energies. Therefore, *the states in the ensemble as a whole describe a continuous band, for both ZnO and TiO*₂ (Figure 3B). The roughly parabolic

shapes reflect the increasing DOS with energy; it is intended to represent the shape of the DOS for the solution. This DOS for the ensemble of colloidal NPs is *not* directly comparable with the DOS in a bulk single crystal of ZnO or TiO₂, in part due to the contributions from the solution properties and proton-coupling, as described in the next section.

The band description in Figure 3B represents the same experimental results as the individual NP picture in Figure 3A and provides additional insights. To describe the particular experiments reported here, the DOS on the TiO₂ vs. ZnO NPs must consider both the individual band pattern (Figure 3A) and the much larger concentration of ZnO NPs in the colloidal suspension. The ~10 times larger number of ZnO NPs means that the number of states in the ZnO ensemble will be ~10 times larger under these reaction conditions than indicated in the narrow ZnO shape in Figure 3B. The DOS for the entire ensemble of ZnO NPs would be similar to that for the TiO₂ NPs. This is why electrons typically flow from TiO₂ to ZnO: because there are so many more ZnO NPs under our conditions. This entropic effect is not captured by the single particle description in Figure 3A.

The complimentary descriptions of the states in TiO₂ and ZnO in Figure 3A and 3B rationalize the experiment results above. The localized nature of the added electrons in TiO₂, likely in a variety of cluster-type trap states, suggests that these states do not strongly interact. Thus, many states can be filled within a small energy range. In contrast, the delocalized electrons in ZnO interact with each other more strongly, resulting in a large energy penalty when another electron is added. For these reasons, TiO₂ can be reduced to a level where formally 8% of all the titanium ions are Ti³⁺, while for ZnO the maximum level is 0.1% of Zn²⁺ (Table 1). Thus, for similarly sized NPs, TiO₂ is inherently much more *reducible* than ZnO. *The higher reducibility reflects the integrated number of states, not the relative band edge energies*.

The qualitative band picture in Figure 3 is affected by several other factors. For example, the size of ZnO is known to affect both the band gap energy and the effective reduction potential. The quantum confinement of the ZnO NPs means that the band gap becomes larger at smaller sizes. 10, 22 In the context of Figure 3, smaller ZnO NPs possess a distribution of states that is narrower and higher in energy than that for larger ones. Smaller ZnO NPs are therefore more difficult to reduce. This is evidenced in the equilibration experiments in which small ZnO NPs are less reduced by TiO₂ (33%) or CoCp*₂ (only by 1 electron). The size dependence of the effective reduction potential of ZnO has also been observed and used in prior studies.²² Overall, this discussion shows that the comparison of multiply charged materials such as ZnO and TiO₂ is complex and nuanced. Understanding the redox chemistry requires another layer of consideration past the band edge, including the number of states electrons may occupy as well.

II. Beyond an electronic density of states model

The "density of states" for a bulk semiconductor refers to the density of purely electronic states. This DOS refers to the states that are present in a chemically fixed material, one that is not undergoing any making or breaking of chemical bonds. However, small colloidal NPs have a high ratio of surface to bulk atoms. When chemical changes occur at the surface, electron energies are affected. In many studies of colloidal NP systems, capping ligands, other properties of the solution, and the chemically complex surface regions alter the redox chemistry of the NPs. 14, 26-27, 46, 55 Our lab and others have previously shown for ZnO nanocrystals that the acid/base character of the solution and the presence of small cations can strongly affect the electronic landscape and the extent of reduction. 12-13, 34, 36 The experiments reported above show that the ET energetics of the ZnO and TiO₂ NPs are affected by the presence of excess capping ligands.

The addition of a large excess of DDA has a small but noticeable effect on a ZnO NC/CoCp*2 suspension, shifting the equilibrium back towards $CoCp^*_2$ from e^-/ZnO . The shift of roughly a factor of 2 corresponds to an electrochemical potential shift of ~20 mV. To obtain this small shift, the DDA concentration was raised from 0.6 mM to 80 mM DDA in solution, an increase of 130-fold. The influence of oleic acid (OL-H) is opposite: CoCp*2 transfers all of its electrons to ZnO NPs when the solution is made 70 mM in OL-H. Similar observations were seen in the TiO₂/CoCp*₂ system (Figure 2B). Addition of 70 mM DDA to an equilibrated TiO₂/CoCp*₂ solution containing 2 mM OL/OL-H resulted in half the electrons on TiO₂ transferring back to CoCp*₂*. However, a 40fold increase in OL-H (to 80 mM) gave a shift in the other direction, with complete transfer of electrons from CoCp*₂ to TiO₂ (See SI, Table 2).

We emphasize that these experiments reflect equilibrium properties rather than kinetic factors. The ligand shells are sufficiently patchy or labile to allow ample access to the NC surfaces. As noted above, these DDA-capped ZnO NPs have \leq 25% surface coverage, with many ligands being very labile. Hedox reactions with small molecules often occur on ms or faster timescales. The reactions of ZnO NPs are typically slowed somewhat by addition of excess DDA, the experiments here have given sufficient time for equilibrium to be reached.

It is perhaps surprising that added DDA and OL-H have opposite effects on the equilibrations with $CoCp^*_2$. However, the capping ligands have different chemical properties: DDA is a base while OL-H is an acid. The effects observed parallel prior results on the addition of acids or bases to ZnO NPs. The addition of [DDA-H][BAr F_4] ([BAr F_4] $^-$ = tetrakis[3,5-bis(trifluoromethyl)-

phenyl]borate) in 1:1 toluene/THF causes a much more substantial shift in the effective reduction potential of ZnO; for instance, the addition of 1 H⁺ led to reduction by roughly 1 e^- from CoCp*2.34-35 The strong P₄-t-Bu phosphazene base shifts the ET equilibrium back toward CoCp*₂. The effects of capping ligands reported here are much smaller, as large amounts of capping ligands shift the CoCp*2/CoCp*2+ equilibria only a small amount. Further differences also likely reflect that DDA is a base and OL-H is an acid. P4-t-Bu phosphazene is a much stronger base than DDA. Cationic [DDA-H][BAr^F₄] is similarly a stronger acid than OL-H in the low-polarity toluene solvent used here^{57-58,35} DDA most likely acts as a hydrogen-bond acceptor for surface hydroxides and withdraws electron density shifting the effective reduction potential. The added OL-H similarly could act as a hydrogen bond donor to surface oxide or hydroxide groups or could convert a surface oxide to a surface hydroxide pair.

The experiments adding OL-H or DDA to equilibrated mixed colloids reveal the *differential* effect of the capping ligands on the TiO_2 and ZnO energetics. These shifts are subtler compared to when NPs are equilibrated with $CoCp^*_2$. The TiO_2 NPs appear to have a greater sensitivity to the added ligands. For instance, added DDA shifts the equilibrium from e^-/TiO_2 to e^-/ZnO , indicating that the basic capping ligand destabilizes the electrons on TiO_2 more than it destabilizes electrons on ZnO. The small effects in these experiments likely also have a contribution from ligand exchange, such as OL binding to ZnO in place of the native DDA. However, since the shifts observed in these experiments were very small, any ligand exchange does not appear to be a major effect.

We have previously suggested that these ZnO and TiO₂ NPs more often behave as proton-coupled electron transfer (PCET) agents than simple ET reagents.⁴⁰ For instance, a phenoxyl radical ArO. is as the titrant for redox equivalents because of its fast conversion to the phenol ArOH. On this general basis, we believe that the interparticle ET reactions are likely PCET processes (Figures 1 and 2 reactions). In addition, multi-electron outer sphere ET between NPs appears very unlikely because it would form multiply charged NPs in non-polar toluene solvent. Still, we have no accessible technique to monitor the protons directly in these reactions. We previously showed that equilibrations with CoCp*2 gave reduced ZnO NPs with tightly ion-paired CoCp*2+.36 The reductions of TiO2 NPs are always done in the presence of OL-H, so these could potentially be PCET processes, or could involve just association of an OL-H molecule.

The shifts in the relative energetics of the ZnO and TiO_2 band energies upon addition of capping ligands show that the energy of the added electrons are affected by the concentration of species in solution. The capping ligands at the surface affect the global energetics of

these reactions, not just a few states. This involvement of the ligands complicates the interpretation of the "density of states" analysis in the previous section. If the addition of an electron to TiO_2 is accompanied by a proton from ZnO or by the binding of a surface OL-H ligand, then the "states" being referred to are not the purely electronic states of the NP. Thus, the DOS schemes in Figure 3 are not directly analogous to standard solid-state densities of electronic states. Perhaps the wide variation in reported absolute E_{CB} values noted in the Introduction are due to the lack of attention to the other species in solution and their potential interactions with the nanomaterials. Efforts to develop a more rigorous analysis of the energetics, including the effects of ligands and protons, are ongoing in our laboratory.

Conclusions

A detailed understanding of the energetics of nanoparticle redox processes is critical to their increasingly widespread use. The experiments described here show that the commonly used simple pictures, such as Scheme 1, are incomplete, especially for materials that undergo substantial electron accumulation. For the colloidal ZnO and TiO₂ NPs examined here, equilibrium studies between the two types of NPs and with CoCp*2 give a direct and detailed experimental view of their electron accumulation. While TiO2 is regarded as a "reducible" oxide and ZnO as "non-reducible", it has long been known that their conduction band edge energies are quite close. The reducibility of the TiO₂ NPs reflects their ability to each accept 30 times more electrons than a ZnO NP. This reflects the much higher density of reducible states in TiO2. Despite an overall preferential flow of electrons from TiO2 to ZnO under our conditions, the most stable e^- in TiO₂ lie lower in energy than the lowest states in ZnO, as not all the electrons can be transferred to ZnO. Additionally, the energetics of charge transfer is affected by capping ligands. Addition of oleic acid or dodecylamine capping ligands shift the equilibria in different directions based on the acid or base properties of the ligands. The energetic landscape of these NPs is thus affected by the nature of the solution they are suspended in, not just the core of the materials. Ultimately, this investigation extends and enriches the traditional discussion that is centered on band edge energies and purely electron transfer frameworks to describe nanomaterial reactivity.

ASSOCIATED CONTENT

Supporting Information. Experimental methods, optical and EPR spectra are available free of charge via http://pubs.acs.org

AUTHOR INFORMATION

Corresponding Author

james.mayer@yale.edu

ACKNOWLEDGMENT

The authors declare no competing financial interests. We thank the U.S. National Science Foundation CHE-1609434 for support of this work. We acknowledge the financial support from NSF as noted above and we thank Professor Gary Brudvig and Dr. David Vinyard for help with our EPR experiments.

REFERENCES

- (1) Ardo, S.; Meyer, G. J., Photodriven heterogeneous charge transfer with transition-metal compounds anchored to TiO₂ semiconductor surfaces. *Chem. Soc. Rev.* **2009**, *38*, 115-164.
- (2) Waite, T. D. In *Geochemical Processes at Mineral Surfaces*; American Chemical Society: 1987; Vol. 323, pp 426-445.
- (3) Nozik, A. J., Photoelectrochemistry: applications to solar energy conversion. *Annu. Rev. Phys. Chem.* **1978**, *29*, 189-222.
- (4) Gratzel, M., Photoelectrochemical cells. *Nature* **2001**, *414*, 338-344
- (5) Morrison, S. R. Electrochemistry at Semiconductor and Oxidized Metal Electrodes; Springer US: 1980.
- (6) Finklea, H. O. In *Semiconductor Electrodes*; Elsevier: Amsterdam, 1988, pp. 43-145.
- (7) Nowotny, J. In *Oxide Semiconductors for Solar Energy: Titanium Dioxide;* CRC press: Boca Raton, 2011, pp 165-206.
- (8) Watson, D. F.; Meyer, G. J., Cation effects in nanocrystalline solar cells. *Coord. Chem. Rev.* **2004**, *248*, 1391-1406.
- (9) Ondersma, J. W.; Hamann, T. W., Conduction band energy determination by variable temperature spectroelectrochemistry. *Energy Environ. Sci.* **2012**, *5*, 9476-9480.
- (10) Enright, B.; Fitzmaurice, D., Spectroscopic determination of electron and hole effective masses in a nanocrystalline semiconductor film. *J. Phys. Chem.* **1996**, *100*, 1027-1035.
- (11) Flood, R.; Fitzmaurice, D., Preparation, characterization, and potential-dependent optical absorption spectroscopy of unsupported large-area transparent nanocrystalline TiO₂ membranes. *J. Phys. Chem.* **1995**, *99*, 8954-8958.
- (12) Brozek, C. K.; Hartstein, K. H.; Gamelin, D. R., Potentiometric titrations for measuring the capacitance of colloidal photodoped ZnO nanocrystals. *J. Am. Chem. Soc.* **2016**, *138*, 10605-10610
- (13) Carroll, G. M.; Brozek, C. K.; Hartstein, K. H.; Tsui, E. Y.; Gamelin, D. R., Potentiometric measurements of semiconductor nanocrystal redox potentials. *J. Am. Chem. Soc.* **2016**, *138*, 4310-4313
- (14) Lyon, L. A.; Hupp, J. T., Energetics of the nanocrystalline titanium dioxide/aqueous solution interface: approximate conduction band edge variations between $H_0 = -10$ and $H_c = +26$. *J. Phys. Chem. B* **1999**, *103*, 4623-4628.
- (15) Lemon, B. I.; Hupp, J. T., Photochemical quartz crystal microbalance study of the nanocrystalline titanium dioxide semiconductor electrode/water interface: Simultaneous photoaccumulation of electrons and protons. *J. Phys. Chem.* **1996**, *100*, 14578-14580.
- (16) Ramamurthy, V. S., K. S.; Gaal, D. A.; Hupp, J. T. *Semiconductor Photochemistry and Photophysics*; Marcel Dekker: New York, 2003; Vol. 10.
- (17) Renault, C.; Nicole, L.; Sanchez, C.; Costentin, C.; Balland, V.; Limoges, B., Unraveling the charge transfer/electron transport in mesoporous semiconductive TiO₂ films by voltabsorptometry. *Phys. Chem. Chem. Phys.* **2015**, *17*, 10592-10607.

- (18) Costentin, C.; Di Giovanni, C.; Giraud, M.; Savéant, J. M.; Tard, C., Nanodiffusion in electrocatalytic films. *Nat. Mater.* **2017**, *16*, 1016-1021.
- (19) Lee, C.Y.; Bond, A. M., Revelation of multiple underlying RuO₂ redox processes associated with pseudocapacitance and electrocatalysis. *Langmuir* **2010**, *26*, 16155-16162.
- (20) Gambardella, A. A.; Bjorge, N. S.; Alspaugh, V. K.; Murray, R. W., Voltammetry of diffusing 2 nm iridium oxide nanoparticles. *J. Phys. Chem. C* **2011**, *115*, 21659-21665.
- (21) Cohn, A. W.; Kittilstved, K. R.; Gamelin, D. R., Tuning the potentials of "extra" electrons in colloidal n-type ZnO nanocrystals via Mg²⁺ substitution. *J. Am. Chem. Soc.* **2012**, *134*, 7937-7943.
- (22) Hayoun, R.; Whitaker, K. M.; Gamelin, D. R.; Mayer, J. M., Electron transfer between colloidal ZnO nanocrystals. *J. Am. Chem. Soc.* **2011**, *133*, 4228-4231.
- (23) Jakob, M.; Levanon, H.; Kamat, P. V., Charge distribution between uv-irradiated TiO₂ and gold nanoparticles: determination of shift in the fermi level. *Nano Lett.* **2003**, *3*, 353-358.
- (24) Roth, A. P.; Webb, J. B.; Williams, D. F., Absorption edge shift in ZnO thin films at high carrier densities. *Solid State Commun.* **1981**, *39*, 1269-1271.
- (25) Whitaker, K. M.; Ochsenbein, S. T.; Polinger, V. Z.; Gamelin, D. R., Electron confinement effects in the EPR spectra of colloidal n-type ZnO quantum dots. *J. Phys. Chem. C* **2008**, *112*, 14331-14335.
- (26) Owen, J., The coordination chemistry of nanocrystal surfaces. *Science* **2015**, *347*, 615-616.
- (27) Thompson, C. M.; Kodaimati, M.; Westmoreland, D.; Calzada, R.; Weiss, E. A., Electrostatic control of excitonic energies and dynamics in a CdS quantum dot through reversible protonation of its ligands. *J. Phys. Chem. Lett.* **2016**, *7*, 3954-3960.
- (28) Anderson, N. C.; Hendricks, M. P.; Choi, J. J.; Owen, J. S., Ligand exchange and the stoichiometry of metal chalcogenide nanocrystals: spectroscopic observation of facile metal-carboxylate displacement and binding. *J. Am. Chem. Soc.* **2013**, *135*, 18536-18548
- (29) De Roo, J.; De Keukeleere, K.; Hens, Z.; Van Driessche, I., From ligands to binding motifs and beyond; the enhanced versatility of nanocrystal surfaces. *Dalton Trans.* **2016**, *45*, 13277-13283.
- (30) Owen, J.; Brus, L., Chemical synthesis and luminescence applications of colloidal semiconductor quantum dots. *J. Am. Chem. Soc.* **2017**, *139*, 10939-10943.
- (31) Jankulovska, M.; Berger, T.; Wong, S. S.; Gómez, R.; Lana-Villarreal, T., Trap states in TiO₂ films made of nanowires, nanotubes or nanoparticles: An electrochemical study. *ChemPhysChem* **2012**, *13*, 3008-3017.
- (32) Morris, A. J.; Meyer, G. J., TiO₂ surface functionalization to control the density of states. *J. Phys. Chem. C* **2008**, *112*, 18224-18231
- (33) Berger, T.; Anta, J. A.; Morales-Flórez, V., Electrons in the band gap: spectroscopic characterization of anatase TiO_2 nanocrystal electrodes under fermi level control. *J. Phys. Chem. C* **2012**, *116*, 11444-11455.
- (34) Valdez, C. N.; Braten, M.; Soria, A.; Gamelin, D. R.; Mayer, J. M., Effect of protons on the redox chemistry of colloidal zinc oxide nanocrystals. *J. Am. Chem. Soc.* **2013**, *135*, 8492-8495.
- (35) Valdez, C. N.; Schimpf, A. M.; Gamelin, D. R.; Mayer, J. M., Proton-controlled reduction of zno nanocrystals: Effects of molecular reductants, cations, and thermodynamic limitations. *J. Am. Chem. Soc.* **2016**, *138*, 1377-1385.
- (36) Valdez, C. N.; Delley, M. F.; Mayer, J. M., Cation effects on the reduction of colloidal ZnO nanocrystals. *J. Am. Chem. Soc.* **2018**, *140*, 8924-8933.
- (37) Cohn, A. W.; Janßen, N.; Mayer, J. M.; Gamelin, D. R., Photocharging ZnO nanocrystals: picosecond hole capture, electron accumulation, and auger recombination. *J. Phys. Chem. C* **2012**, *116*, 20633-20642.
- (38) Schimpf, A. M.; Gunthardt, C. E.; Rinehart, J. D.; Mayer, J. M.; Gamelin, D. R., Controlling carrier densities in photochemically

- reduced colloidal ZnO nanocrystals: size dependence and role of the hole quencher. J. Am. Chem. Soc. 2013, 135, 16569-16577.
- (39) Schouteden, K.; Zeng, Y. J.; Lauwaet, K.; Romero, C. P.; Goris, B.; Bals, S.; Van Tendeloo, G.; Lievens, P.; Van Haesendonck, C., Band structure quantization in nanometer sized ZnO clusters. *Nanoscale* **2013**, *5*, 3757-3763.
- (40) Schrauben, J. N.; Hayoun, R.; Valdez, C. N.; Braten, M.; Fridley, L.; Mayer, J. M., Titanium and zinc oxide nanoparticles are proton-coupled electron transfer agents. *Science* **2012**, *336*, 1298-1301.
- (41) Meulenkamp, E. A., Synthesis and growth of ZnO nanoparticles. J. Phys. Chem. B 1998, 102, 5566-5572.
- (42) Cozzoli, P. D.; Kornowski, A.; Weller, H., Low-temperature synthesis of soluble and processable organic-capped anatase TiO₂ nanorods. *J. Am. Chem. Soc.* **2003**, *125*, 14539-14548.
- (43) Meulenkamp, E. A., Size dependence of the dissolution of ZnO nanoparticles. *J. Phys. Chem. B* **1998**, *102*, 7764-7769.
- (44) Valdez, C. N.; Schimpf, A. M.; Gamelin, D. R.; Mayer, J. M., Low capping group surface density on zinc oxide nanocrystals. *ACS Nano* **2014**, *8*, 9463-9470.
- (45) Fritzinger, B.; Capek, R. K.; Lambert, K.; Martins, J. C.; Hens, Z., Utilizing self-exchange to address the binding of carboxylic acid ligands to CdSe quantum dots. *J. Am. Chem. Soc.* **2010**, *132*, 10195-10201.
- (46) Cass, L. C.; Malicki, M.; Weiss, E. A., The chemical environments of oleate species within samples of oleate-coated PbS quantum dots. *Anal. Chem.* **2013**, *85*, 6974-6979.
- (47) Kalyanasundaram, K.; Grätzel, M.; Pelizzetti, E., Interfacial electron transfer in colloidal metal and semiconductor dispersions and photodecomposition of water. *Coord. Chem. Rev.* **1986**, *69*, 57-125.
- (48) Carroll, G. M.; Schimpf, A. M.; Tsui, E. Y.; Gamelin, D. R., Redox potentials of colloidal n-type ZnO nanocrystals: Effects of confinement, electron density, and fermi-level pinning by aldehyde hydrogenation. *J. Am. Chem. Soc.* **2015**, *137*, 11163-11169.
- (49) Ghosh, A. K.; Wakim, F. G.; Addiss, R. R., Photoelectronic processes in rutile. *Phys. Rev.* **1969**, *184*, 979-988.
- (50) Peper, J. L.; Vinyard, D. J.; Brudvig, G. W.; Mayer, J. M., Slow equilibration between spectroscopically distinct trap states in reduced TiO₂ nanoparticles. *J. Am. Chem. Soc.* **2017**, *139*, 2868-2871.
- (51) Howe, R. F.; Gratzel, M., EPR observation of trapped electrons in colloidal titanium dioxide. *J. Phys. Chem.* **1985**, *89*, 4495-4499.
- (52) Chiesa, M.; Paganini, M. C.; Livraghi, S.; Giamello, E., Charge trapping in TiO₂ polymorphs as seen by electron paramagnetic resonance spectroscopy. *Phys. Chem. Chem. Phys.* **2013**, *15*, 9435-
- (53) Shim, M.; Guyot-Sionnest, P., N-type colloidal semiconductor nanocrystals. *Nature* **2000**, *407*, 981-983.
- (54) Roest, A. L.; Kelly, J. J.; Vanmaekelbergh, D.; Meulenkamp, E. A., Staircase in the electron mobility of a ZnO quantum dot assembly due to shell filling. *Phys. Rev. Lett.* **2002**, *89*, 036801.
- (55) Henckel, D. A.; Lenz, O.; Cossairt, B. M., Effect of ligand coverage on hydrogen evolution catalyzed by colloidal SWe₂. *ACS Catal.* **2017**, *7*, 2815-2820.
- (56) Braten, M. N.; Gamelin, D. R.; Mayer, J. M., Reaction dynamics of proton-coupled electron transfer from reduced ZnO nanocrystals. *ACS Nano* **2015**, *9*, 10258-10267.
- (57) Schwesinger, R.; Schlemper, H.; Hasenfratz, C.; Willaredt, J.; Dambacher, T.; Breuer, T.; Ottaway, C.; Fletschinger, M.; Boele, J.; Fritz, H.; *et al.*, Extremely strong, uncharged auxiliary bases; monomeric and polymer-supported polyaminophosphazenes (p2–p5). *Liebigs Annalen* **1996**, *1996*, 1055-1081.
- (58) Schwesinger, R.; Schlemper, H., Peralkylated polyaminophosphazenes extremely strong, neutral nitrogen bases. *ACIEE* **1987**, *26*, 1167-1169.

TOC GRAPHIC

